CALCULATION OF SHOCK-SEPARATED TURBULENT BOUNDARY LAYERS

By B. S. Baldwin and W. C. Rose
NASA Ames Research Center

12

SUMMARY

Numerical solutions of the complete, time-averaged conservation equations using several eddy-viscosity models for the Reynolds shear stress to close the equations are compared with experimental measurements in a compressible, turbulent separated flow. An efficient time-splitting, explicit difference scheme was used to solve the two-dimensional conservation equations. The experiment used for comparison was a turbulent boundary layer that was separated by an incident shock wave in a Mach 2.93 flow with a unit Reynolds number of 5.7×10^7/m. Comparisons of predicted and experimental values of surface pressure, shear stress along the wall, and velocity profiles are shown. One of the tested eddy-viscosity models which allows the shear stress to be out of equilibrium with the mean flow produces substantially better agreement with the experimental measurements than the simpler models. A tool is thereby provided for inferring additional information about the flow, such as static pressures in the stream, which might not be directly obtainable from experiments.

INTRODUCTION

Development of turbulence models capable of adequately predicting separated compressible flows requires extensive comparisons of calculations with a variety of experiments. At present, the proper role of the calculations is perhaps to aid in the design, interpretation, and documentation of the experiments. For those purposes, it is expedient to seek simple empirical relationships that can be used in the calculations to correlate the experiments. Only after a reliable body of experimental data has been accumulated will definitive verification of the advanced turbulence models be possible.

The adequacy of the numerical method for solving the conservation equations has been established by comparison of calculations with experimental measurements in laminar separated flows (refs. 1 to 3). Methods and procedures for incorporating turbulence models efficiently in the numerical methods are still in a stage of development. Thus, while experience is being gained with these methods and procedures, it is expedient to utilize simple empirical relationships in most of the calculations rather than add the complication of advanced turbulence models.

Several solutions to the conservation equations for compressible turbulent separated flows have been obtained to date (refs. 4 to 8). The present investigation was motivated and guided by interaction with experiments conducted by the authors of references 9 to 11. The class of experiments considered in this study (i.e., non-hypersonic, near-adiabatic wall condition) was chosen for examination to minimize uncertainty with the body of data to be used for comparison with the calculations. In addition, the effects of pressure fluctuations which might influence the turbulence modeling are minimized in such flows. An attempt has been made in the present study to find modifications of a simple algebraic turbulence model that will adequately represent the turbulent shear stress throughout a shock-separated turbulent boundary layer.

SYMBOLS

C_f	skin-friction coefficient $\left(\frac{\tau_w}{0.5 \rho_\infty u_\infty^2}\right)$
C_p	pressure coefficient
ℓ	mixing length
M	Mach number
p	pressure
Pr	Prandtl number (0.72)
Pr_T	turbulent Prandtl number (0.9)
Re	Reynolds number
T	temperature
u	streamwise velocity
u_{max}	maximum velocity in boundary layer
u_τ	friction velocity
v	velocity in y-direction

x	streamwise coordinate
x_i	inviscid impingement location
y	cross-stream coordinate
δ	boundary-layer thickness
ϵ	eddy viscosity
ϵ_{inner}	eddy viscosity near wall
ϵ_{outer}	eddy viscosity in outer part of boundary layer
μ	absolute viscosity
ρ	density
τ_{xy}	shear stress fluxes in Navier-Stokes equations
τ	total shear stress, $-\tau_{xy}$

Subscripts:

e	edge of boundary layer
o	upstream conditions
t	total conditions
w	wall conditions
∞	free-stream conditions

Superscript:

+	indicates dimensionless boundary-layer quantity

PRELIMINARY CONSIDERATIONS

Description of the Flow

The flow field considered in this study is shown schematically in figure 1. (See ref. 10 for complete detail.) The free-stream Mach number is 2.93 and the unit Reynolds number is 5.7×10^7/m. A shock wave, generated by a plate set at 13° to the free stream, impinges on the turbulent boundary layer at the upper nozzle wall. This incident and reflected shock system produces a large pressure rise $\left(p_{final}/p_{initial} \approx 5\right)$ and causes the boundary layer to separate. The pressure rise feeds upstream in the subsonic part of the boundary layer and forms a separation bubble containing reversed flow; hence, separation occurs well upstream of the inviscid shock impingement point. An induced shock wave results from the upstream separation and a reflected shock wave also forms. Although care was taken in the experiment to minimize three-dimensional effects, the flow may still contain these effects as noted in reference 10. This is important to consider since the present numerical method applies strictly to two-dimensional flows.

The Numerical Method

The time-averaged Navier-Stokes equations to be solved are listed in reference 5. The numerical method and special numerical procedures used in the calculations presented herein are described in detail in references 2 and 5. The grid used in the present study had 40 nodes in the streamwise direction with $\Delta x = 5.1 \times 10^{-3}$ m and 32 nodes in the cross-stream direction with four different Δy ranging from 2.5×10^{-5} m near the wall to 4.8×10^{-3} m beyond the boundary-layer edge.

A simplified turbulence model used previously (refs. 5 to 7) to gain experience in the numerical solutions while conserving computer time expresses the shear stress as

$$\tau_{xy} = -(\mu + \rho\epsilon)\left(\frac{\partial u}{\partial y} + \frac{\partial v}{\partial x}\right) \tag{1}$$

The eddy viscosity ϵ is modeled in two regions within the boundary layer, the inner region comprising essentially the logarithmic region near the wall and the outer region that consists of the wake or approximately the remaining 75 to 80 percent of the boundary layer. In the inner region, a mixing length formulation for the eddy viscosity is used

$$\epsilon_{inner} = \ell^2\left|\frac{\partial u}{\partial y} + \frac{\partial v}{\partial x}\right| \tag{2}$$

where

$$\ell = ky\left[1 - \exp\left(\frac{-y}{A}\right)\right] \tag{3}$$

with

$$A = A_w^+ \frac{\mu_w}{\sqrt{|\tau_w|\rho_w}} \tag{4}$$

$k = 0.4$, and $A_w^+ = 26$. In the outer region the eddy viscosity is represented by

$$\epsilon_{outer} = 0.0168 \frac{u_{max}\delta_i^*}{I} \tag{5}$$

where

$$\delta_i^* = \int_0^{\delta_o} \left(1 - \frac{u}{u_{max}}\right) dy \tag{6}$$

and

$$I = 1 + \left(\frac{y}{\delta_o}\right)^6 \tag{7}$$

In the calculations, ϵ_{inner} is used in the boundary layer until y is large enough that $\epsilon_{inner} > \epsilon_{outer}$, at which point and beyond ϵ_{outer} is used. The heat flux vector is approximated by

$$\vec{q} = -\left(\frac{\mu}{Pr} + \frac{\rho\epsilon}{Pr_T}\right) C_p \vec{\nabla} T \tag{8}$$

with $Pr = 0.72$ and $Pr_T = 0.9$. The model described in equations (2) to (8) is denoted in the remainder of this paper as the "baseline model."

In addition to the baseline model, various other models or variations of the baseline model were investigated. Calculations using these various models will be described in the "Results and Discussion" section.

The calculations were started at a streamwise station $(x - x_i)/\delta_o = -5.47$ using the experimental turbulent boundary-layer velocity profiles and other information, such as shock-wave location, that is consistent with the experiment. To indicate the resolution of the near-wall region of the boundary layer achieved in the numerical solution, a law of the wall velocity profile is shown in figure 2. The symbols are at the computational mesh points and, as can be seen, at least one point is in the laminar sublayer where $u^+ = y^+$. The flow-field quantities at the mesh points were found by interpolating experimental data. Below the region where experimental data were available (y^+ less than about 500), the quantities were found by setting $\tau = \tau_w$, neglecting streamwise derivatives in the numerical solution using the baseline turbulence model, and constraining the velocity profile to pass through the experimental data beyond $y^+ = 500$. The skin-

friction coefficient $C_f = 1.30 \times 10^{-3}$ calculated in this manner is in close agreement with the experimentally determined value obtained using a Preston tube (ref. 10) and with that obtained from examination of the velocity profile (ref. 12).

RESULTS AND DISCUSSION

Comparison of Baseline Model With Experimental Results

The experimental results of reference 10 are compared with calculations using the baseline model in figures 3 to 6. Figure 3 contains a comparison of experimental and calculated wall pressures as a function of the streamwise coordinate employed in reference 10, namely $(x - x_i)/\delta_o$. Agreement between experiment and theory using the baseline model is poor. In figure 4 the computed skin-friction coefficient is compared with that obtained from velocity profiles from reference 10 analyzed by the method of reference 12. The separation and reattachment points deduced from surface oil-flow observations (ref. 10) are also indicated. Not only is the forward extent of the separation underestimated by the baseline-model calculation but the rearward extent is overestimated. As a result of the apparent inability of the baseline model to describe the observed variation of pressure and skin-friction coefficient, various modifications to that model were made.

Pressure Gradient Modification

To allow for effects of pressure gradients, Cebeci (ref. 13) recommends (in effect) replacement of $A_w^+ = 26$ in equation (4) with

$$A_w^+ = 26\left(1 + 11.8\,\frac{\rho_w}{\rho_e}^{1.5}\,\frac{\mu_e}{\rho_e}\,\frac{dp/dx}{\tau^{1.5}}\right)^{-1/2} \tag{9}$$

where in the present study $\tau = \tau_w + y(\partial p/\partial x)$ (ref. 13) while the eddy viscosity in the outer flow remains unchanged. According to Cebeci, the above correction factor is applicable in the presence of favorable as well as unfavorable pressure gradients. In the present application the modification increases the eddy viscosity in regions ahead of the separation as well as aft of reattachment.

The effect of the Cebeci modification on skin friction is shown in figure 5. The separation bubble is moved slightly forward in the direction of the experiment, but the bubble is also extended farther rearward worsening the agreement with the measurements. Clearly some modification other than that of Cebeci (or in addition to) is needed for the class of separated flows considered here.

Escudier Formulation

An alternative to equation (5) of the baseline model that has been used for attached flows (ref. 14) is

$$\epsilon_{outer} = \ell_{max}^2 \left| \frac{\partial u}{\partial y} + \frac{\partial v}{\partial x} \right|$$

with $\ell_{max} = 0.09\delta$. Results of using the Escudier model are shown also in figure 5. The model, however, is difficult to apply in the present calculation since the local width of the boundary layer δ cannot be defined accurately enough in the numerical calculation because of velocity gradients introduced by curvature of the incident, induced, and reflected shock waves. Slight changes in the definition of δ can change its value by more than a factor of 2. However, as observed in the experiment, the values of δ do not change significantly from the upstream value ahead of the separation. Accordingly, ℓ_{max} based on the upstream boundary-layer thickness $\left(\ell_{max} = 0.09\delta_o\right)$ has been used in several calculations to be described. Figure 6 shows calculated profiles of $\rho\epsilon$ in the separated region according to the baseline model and the Escudier formula. Although, as is well known, the two formulations produce similar variations for attached flows with small pressure gradients, they appear to produce greatly different variations for the present separated flow.

Applying the Escudier formulation in the present calculations greatly reduced the extent of the separation along the wall. As evident in figure 5, the prediction of upstream influence was substantially worse than that of the baseline model, although the rearward extent of the bubble agreed better with indications from oil flow in the experiment. Despite the poor overall agreement shown, the Escudier model can be used as a guide in modifying the turbulence model. The better agreement with reattachment location indicates one type of modification to the turbulence model needed to obtain better agreement with the experimental data. Namely, relative to the baseline model, larger values of eddy viscosity are needed near reattachment to confine the rearward extent of the bubble. However, smaller values are probably needed near separation to promote the proper upstream influence. A model is now discussed that, in fact, does possess these characteristics.

Modification to Account for Nonequilibrium Effects

For separated supersonic flow over a compression corner Shang and Hankey (ref. 8) have obtained remarkably good agreement with experiment by use of a simple modification of an algebraic turbulence model of the form (in the present notation)

$$\rho\epsilon = (\rho\epsilon)_o + \left[(\rho\epsilon)_{equilibrium} - (\rho\epsilon)_o\right] \left\{1 - \exp\left[\frac{-\alpha(x - x_o)}{\delta_o}\right]\right\} \tag{10}$$

with $\alpha = 1/10$. This type of modification (with $\alpha = 1/10$) has been proposed by many authors and has been shown by Rose and Johnson (ref. 11) to agree generally with the values of ℓ_{max} deduced from direct measurements of the Reynolds shear stress. A value of α between 1/5 and 1/15 is consistent with experimental observations, as noted in reference 11.

Application of equation (10) in the present problem with $\alpha = 1/10$ led to results (not shown) similar to those obtained from the Cebeci viscous sublayer modification. Namely (relative to the baseline model), the upstream influence was improved, but the bubble was also extended far downstream in gross disagreement with the experiment.

The observed effects of various turbulence models on the calculations described so far led to the following attempt to model the turbulent shear stress. A formula like equation (10) should apply only to the flow outside the separation bubble since there probably should be no upstream history passing through the front of the bubble (i.e., the turbulence within the bubble is in local equilibrium). In the present study, equilibrium within the bubble was insured by applying equation (10) only if $(\rho\epsilon)_{equilibrium}$ exceeded $(\rho\epsilon)_o$ which does, in fact, allow a local equilibrium condition to prevail in the separation bubble. Since the Escudier formula produces the large values of eddy viscosity needed to limit the rearward extent of the bubble, $(\rho\epsilon)_{equilibrium}$ is determined from that formulation. For the same reason in the present case, a value of $\alpha = 1/5$ was found to be better than $\alpha = 1/10$. In other words the baseline model is modified by the use of equation (10) with

$$\alpha = \begin{cases} \infty & \text{if } (\rho\epsilon)_{equilibrium} < (\rho\epsilon)_o \\ 1/5 & \text{otherwise} \end{cases} \tag{11}$$

where $(\rho\epsilon)_{equilibrium}$ is determined from

$$(\rho\epsilon_{outer})_{equilibrium} = \ell_{max}^2 \left| \frac{\partial u}{\partial y} + \frac{\partial v}{\partial x} \right|$$

$$\ell_{max} = 0.09\delta_o$$

and $(\rho\epsilon_{inner})_{equilibrium}$ from equations (2) to (4) of the baseline model if $\ell < \ell_{max}$. Profiles of $\rho\epsilon$ produced by these modifications are compared with those from the baseline model in figure 7. The desired variation in the values of $\rho\epsilon$ is obtained; that is, upstream near separation $\rho\epsilon$ is lower than the baseline model and downstream near reattachment $\rho\epsilon$ is higher.

In figure 8, calculated wall pressure distributions are compared to the experimental measurements. The upstream influence predicted by the relaxation model is in better agreement with the measurements than the prediction from the baseline or Escudier

models. However, the wall shear stresses shown in figure 9 indicate that prediction of the reattachment point is still poor. Velocity profiles near the front of the bubble predicted by the baseline, relaxation, and Escudier models are compared with measurements in figure 10. Again, the results using the relaxation model are in much better agreement with the data than the simpler models.

Finally, locations of the experimental shock waves and expansion from a tracing of a schlieren photograph of the flow field are compared in figure 11 with the locations of the shocks and expansion predicted using the relaxation model. The good agreement shown for the relaxation model would not be obtained by any other turbulence models investigated in the present study since none of the other models predict the proper upstream influence. One can thus conclude that the flow-field properties, such as regions of shock waves and expansions, can be adequately predicted when a valid turbulence model is used.

CONCLUDING REMARKS

The complete, time-averaged conservation equations have been numerically solved using several algebraic turbulence models. Information has been gained on the effects of the various turbulence models applied to a separating and reattaching compressible turbulent boundary layer. The information has led to the formulation of a relaxation model for the Reynolds shear stress that produces reasonable agreement with a set of experimental data.

REFERENCES

1. MacCormack, R. W.: Numerical Solution of the Interaction of a Shock Wave With a Laminar Boundary Layer. Lecture Notes in Physics, vol. 8, Springer-Verlag, New York, 1971, p. 151.

2. MacCormack, R. W.; and Baldwin, B. S.: A Numerical Method for Solving the Navier-Stokes Equations With Application to Shock-Boundary Layer Interactions. AIAA Paper 75-1, 1975.

3. Hung, C. M.; and MacCormack, R. W.: Numerical Solutions of Supersonic and Hypersonic Laminar Flows Over a Two-Dimensional Compression Corner. AIAA Paper 75-2, 1975.

4. Wilcox, D. C.: Calculation of Turbulent Boundary Layer Shock Wave Interaction. AIAA J., vol. 11, no. 4, 1973, pp. 1592-1594.

5. Baldwin, B. S.; and MacCormack, R. W.: Numerical Solution of the Interaction of a Strong Shock Wave With a Hypersonic Turbulent Boundary Layer. AIAA Paper 74-558, 1974.

6. Deiwert, G. S.: Numerical Simulation of High Reynolds Transonic Flows. AIAA Paper 74-603, 1974.

7. Horstman, C. C.; Kussoy, M. I.; Coakley, T. J.; Rubesin, M. M.; and Marvin, J. G.: Shock-Wave-Induced Turbulent Boundary-Layer Separation at Hypersonic Speeds. AIAA Paper 75-3, 1975.

8. Shang, J. S.; and Hankey, W. L., Jr.: Numerical Solution of the Navier-Stokes Equations for Supersonic Turbulent Flow Over a Compression Corner. AIAA Paper 75-4, 1975.

9. Rose, W. C.: The Behavior of a Compressible Turbulent Boundary Layer in a Shock-Wave Induced Adverse Pressure Gradient. Ph. D. Thesis, Univ. of Washington, 1972. (Available as NASA TN D-7092, 1973.)

10. Reda, D. C.; and Murphy, J. D.: Shock Wave – Turbulent Boundary Layer Interactions in Rectangular Channels, Part II: The Influence of Sidewall Boundary Layers on Incipient Separation and Scale of the Interaction. AIAA Paper 73-234, 1973.

11. Rose, W. C.; and Johnson, D. A.: A Study of Shock-Wave Turbulent Boundary Layer Interaction Using Laser Velocimeter and Hot-Wire Anemometer Techniques. AIAA Paper 74-95, 1974.

12. Rubesin, M. W.; Murphy, J. D.; and Rose, W. C.: Wall Shear in Strongly Retarded and Separated Compressible Turbulent Boundary Layers. AIAA J., vol. 12, no. 10, Oct. 1974, pp. 1442-1444.

13. Cebeci, T.: Calculation of Compressible Turbulent Boundary Layers With Heat and Mass Transfer. AIAA J., vol. 9, no. 6, 1971, pp. 1091-1097.

14. Launder, B. E.; and Spalding, D. B.: Lectures in Mathematical Models of Turbulence. Academic Press, New York, 1972.

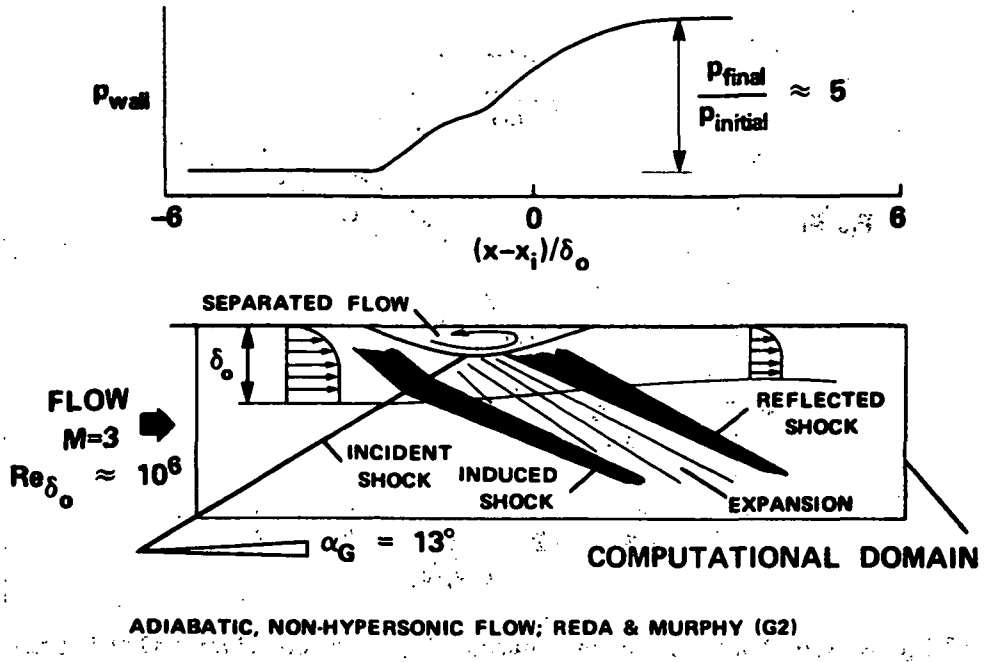

Figure 1.- Schematic drawing of flow field to be calculated.

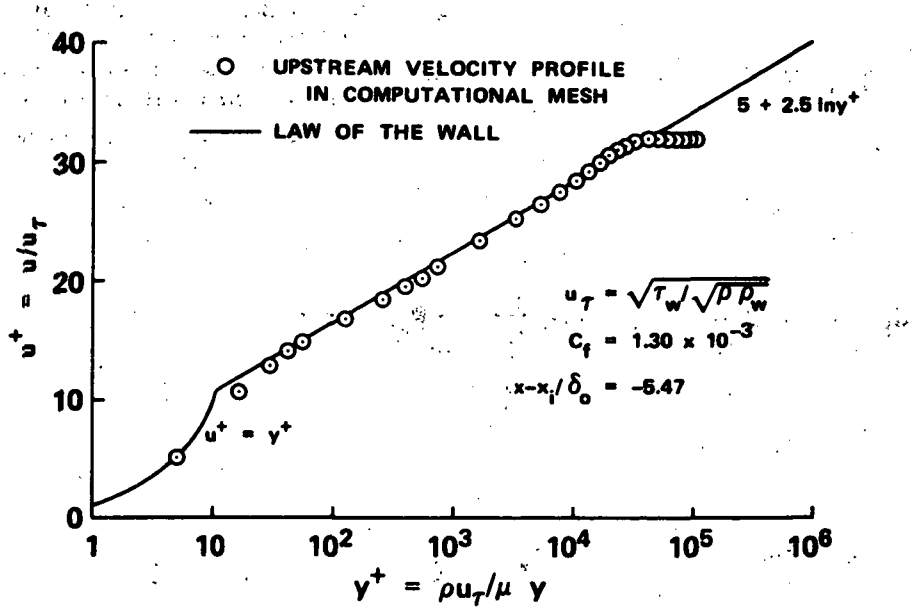

Figure 2.- Upstream velocity profile in law of the wall coordinates.

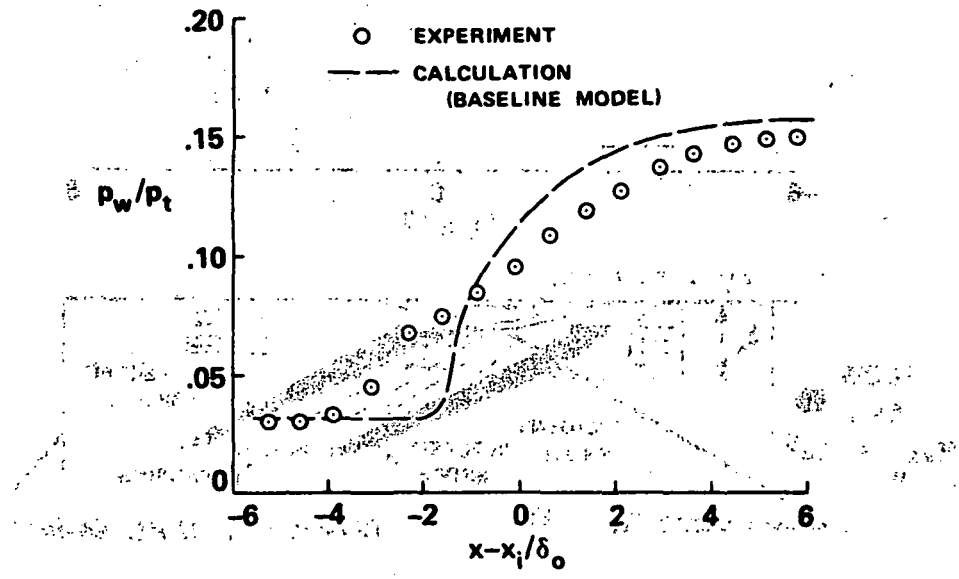

Figure 3.- Comparison of measured pressure with calculation.

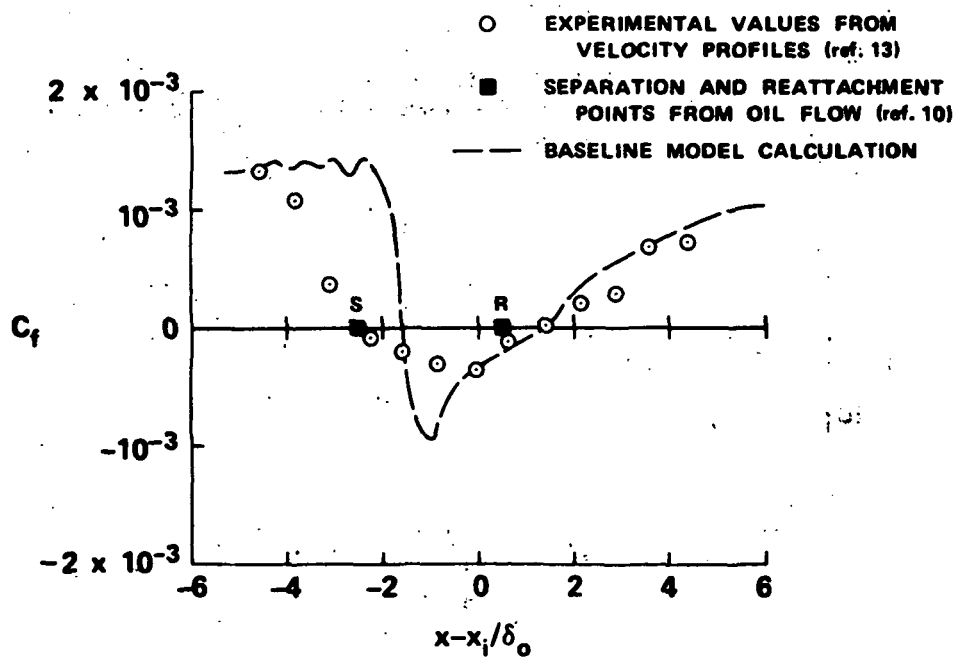

Figure 4.- Comparison of predicted and experimental skin-friction coefficients using baseline model.

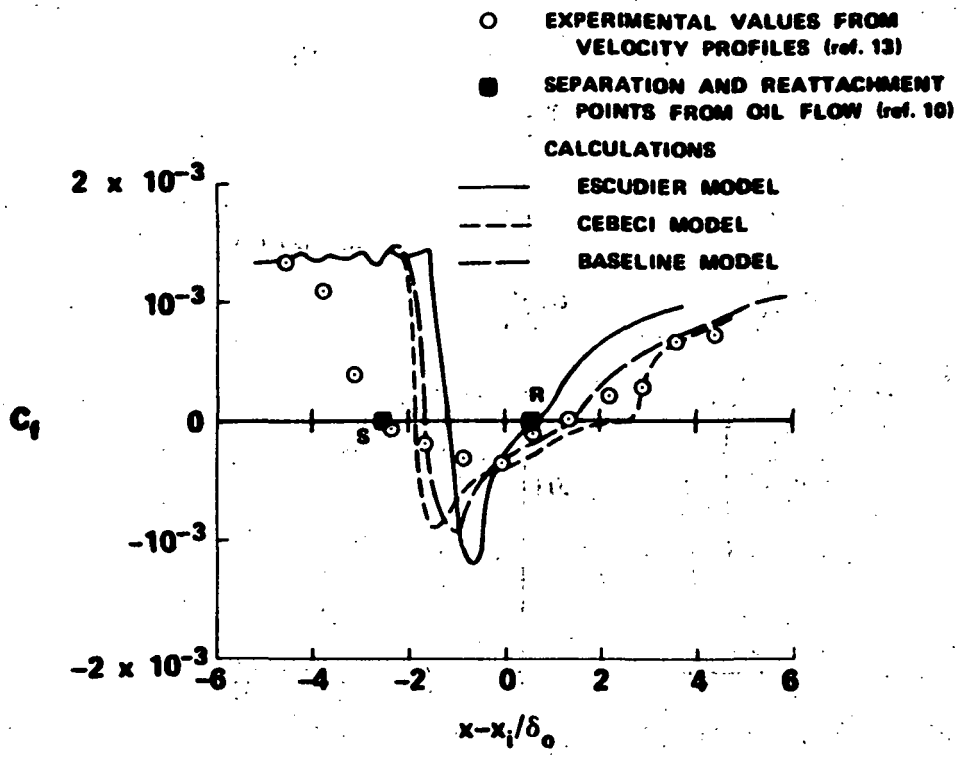

Figure 5.- Comparison of predicted and experimental skin-friction coefficients using various models.

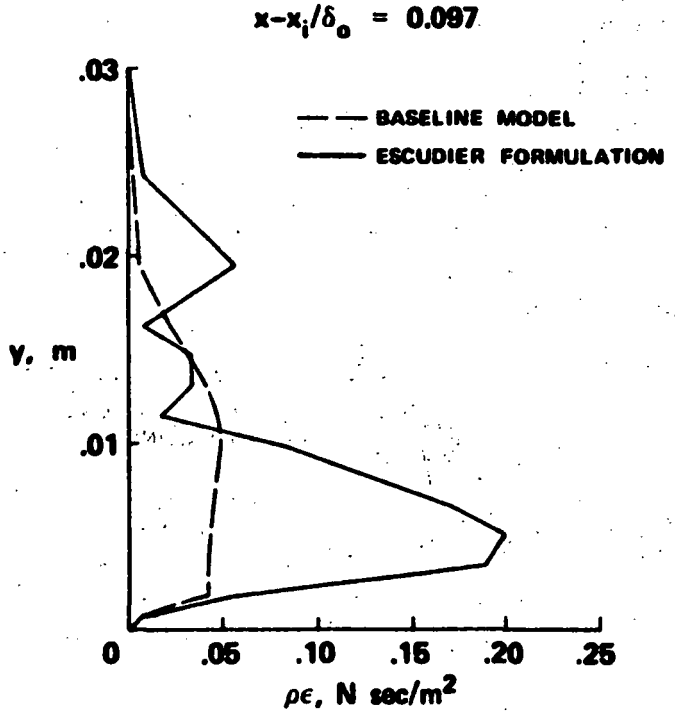

Figure 6.- Comparison of Escudier and baseline eddy-viscosity profiles in separation region.

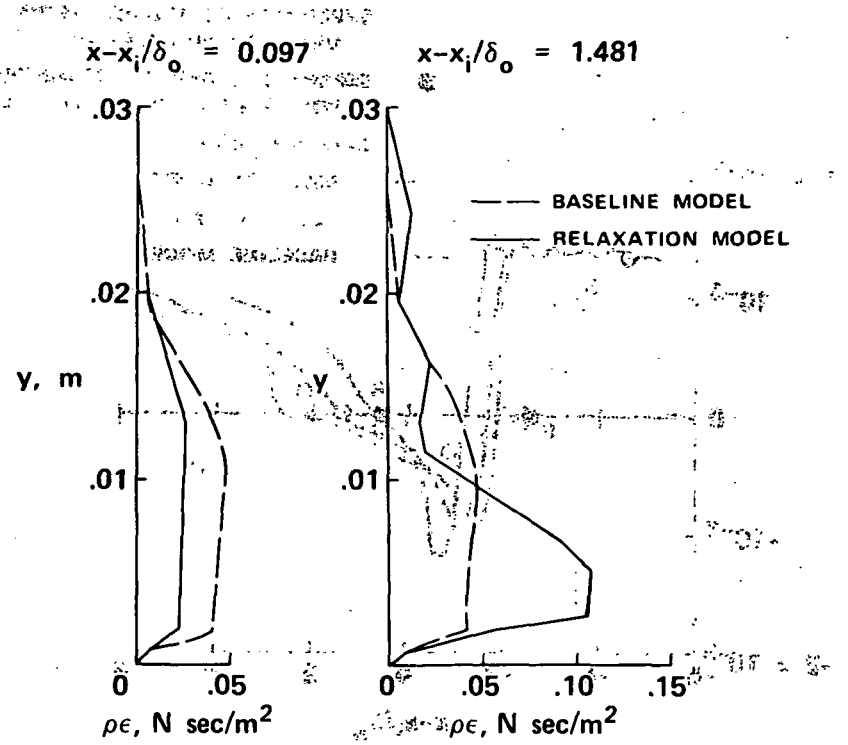

Figure 7.- Comparison of relaxation and baseline eddy-viscosity profiles.

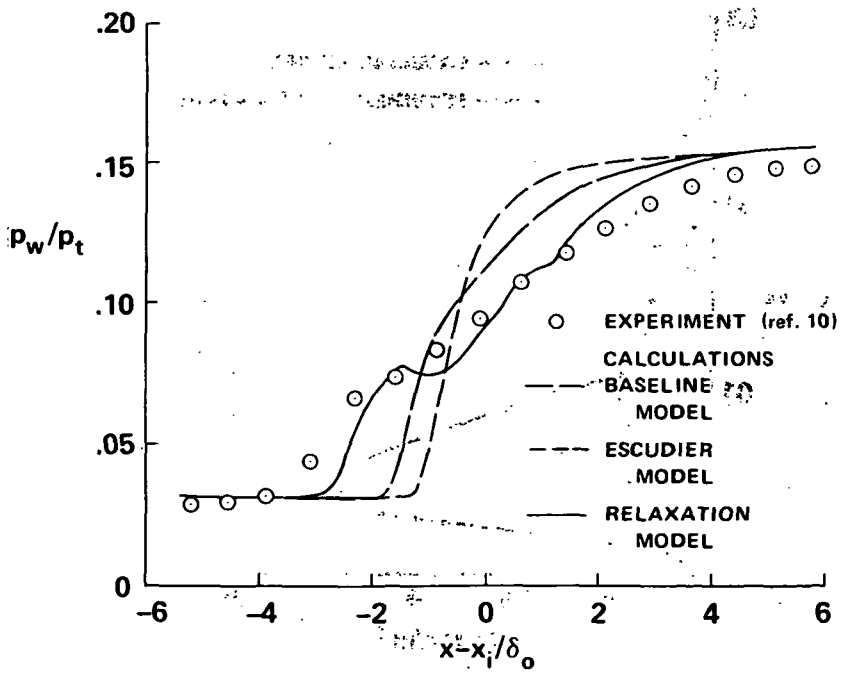

Figure 8.- Comparison of surface static-pressure distributions using various models.

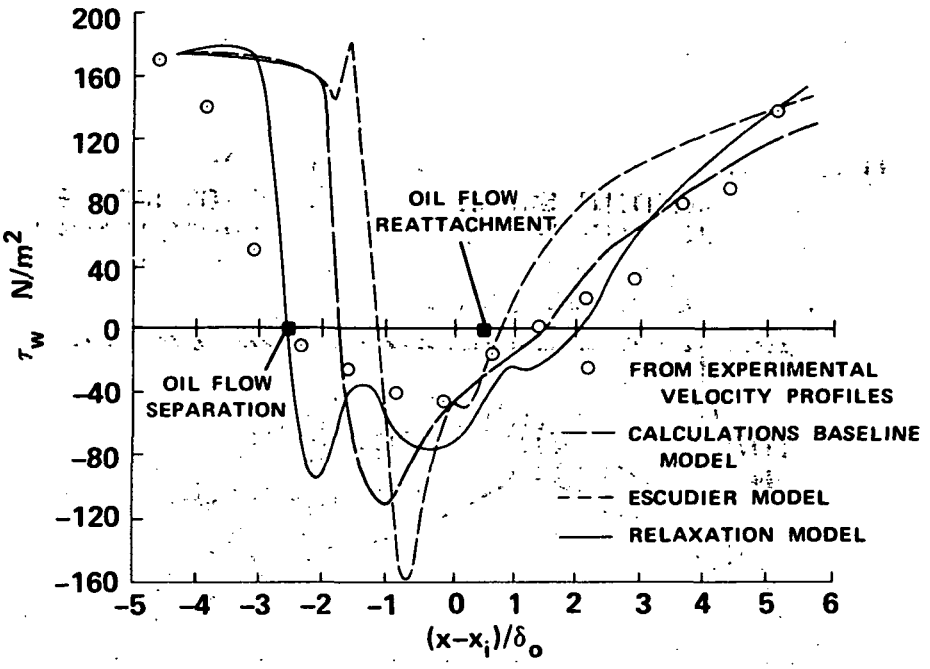

Figure 9.- Comparison of predicted and experimental wall shear stress using various models.

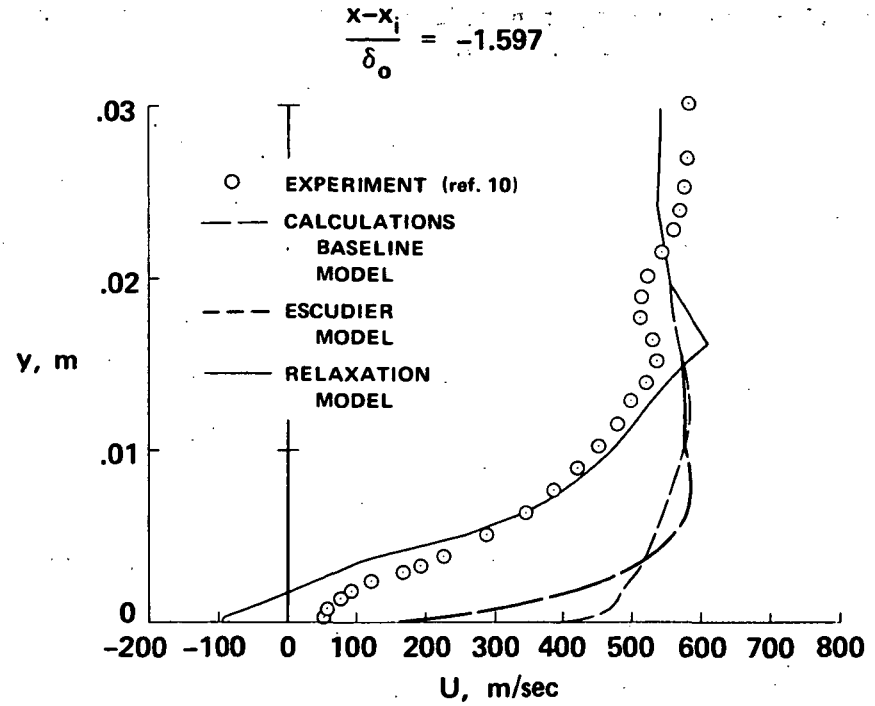

Figure 10.- Comparison of predicted and experimental velocity profiles in separation region.

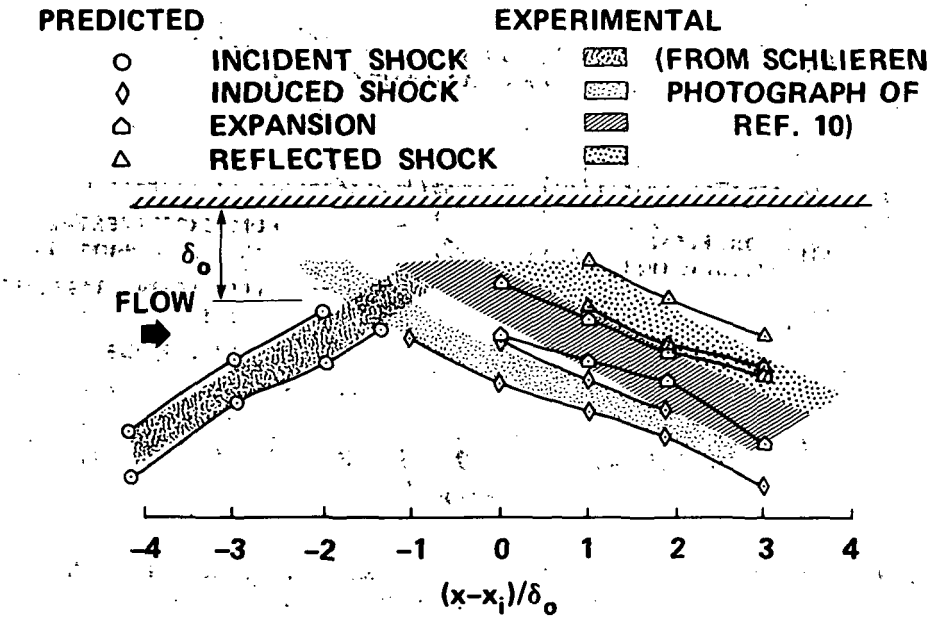

Figure 11.- Comparison of predicted and experimental flow fields using relaxation model.